

CHAPTER 76

AN INVESTIGATION OF THE WAVE FORCES ACTING ON BREAKWATER HANDRAILS

Atsushi HUIJI¹, Shigeo TAKAHASHI² and Kimihiko ENDOH³

ABSTRACT

We carried out model experiments to quantitatively elucidate the motion of overtopping waves on a caisson breakwater, with results leading to the development of an empirical model that can evaluate the maximum current velocity and depth of such waves on a breakwater. In addition, we developed a formula for calculating the wave forces acting on breakwater handrails, then confirmed its validity using field experiments.

1. INTRODUCTION

Seawalls and breakwaters are ideal locations from which people can comfortably enjoy a seafront environment. In Japan, such structures allowing public access are called promenade seawalls or breakwaters. Because such facilities are a dangerous place for personnel, thorough safety measures must be in place before opening them to the public. Handrails installed on seawalls and breakwaters are a basic safety feature, being present on almost all of Japan's promenade facilities.

Many facilities, however, have been damaged by high overtopping waves; thereby creating serious problems for facility safety management. **Figure 1** shows a photograph of damaged promenade breakwater handrails. Obviously then, overtopping wave forces are a major consideration in handrail design, yet only a limited amount of associated quantitative information is available. In addition to determining the wave forces acting on handrails, the motion of overtopping waves must also be clarified.



Figure 1 Photograph of damaged breakwater handrails

1 Niigata Investigation and Design Office, the First District Port Construction Bureau, MOT, 1-332 Hakusan-ura, Niigata 951, Japan

2 Maritime Structures Laboratory, Port and Harbour Research Institute, MOT

3 Port and Harbor Engineering Section, Civil Engineering Research Institute, HDA

This led to the present study which uses laboratory model experiments to (i) examine the characteristics of overtopping waves above a breakwater and (ii) develop a formula for obtaining wave forces acting against a handrail. We also examine the characteristics of wave forces on handrails, then verify the proposed formula using field experiments.

2. MOTION OF OVERTOPPING WAVES ON A CAISSON

2.1 Experiment Outline

To examine the basic characteristics of overtopping wave motion on a composite breakwater, and to develop a model of the motion, we conducted a laboratory model experiment using relatively low wave heights. During this experiment (Experiment A), a 163-m-long, 1-m-wide, and 1.5-m-deep wave flume was employed to measure water depths and current velocities above a model caisson.¹⁾

We also conducted another laboratory experiment using relatively high wave heights over other types of model breakwaters; hence enabling the development of an empirical formula. During this experiment (Experiment B), a 38-m-long, 1-m-wide, and 1.5-m-deep wave flume was employed to measure water depths and current velocities above composite breakwaters, breakwaters covered with wave-dissipating blocks, and slit-caisson breakwaters. Wave forces acting on model handrails were also measured.²⁾

This paper primarily reports on the fundamental motion characteristics of overtopping waves (Experiment A).

2.2 Overtopping Wave Motion

Figure 2 shows overtopping wave motion above a caisson at $hc/H = 0.293$, $H/L = 0.051$, and $\Delta t = 0.05$, being obtained using a high-speed video camera that records 200 frames/s. Note that after the water level in front of the breakwater rises and the wave grows higher than the crown, its shape gradually shifts toward the crown's landward edge. The overtopping wave then crashes on the breakwater, being transformed into one-directional landward flow. We classify these phenomena into the following two stages:

- 1) "Green wave stage": the phenomena occurring from the wave's run-up above the crown to its crash onto it.
- 2) "Overtopping flow stage": the phenomena occurring when the crashed overtopping wave is transformed into fast, landward-directed flow.

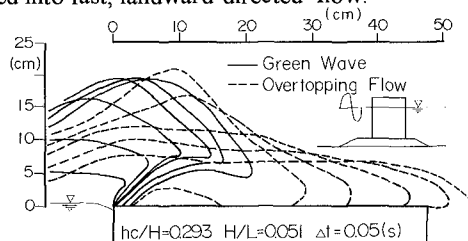


Figure 2 Overtopping wave motion above a caisson

3. OVERTOPPING WAVE MODEL

Figure 3 shows a diagram representing the "overtopping wave model (OWM)," which we apply to empirically evaluate the maximum water depth and current velocity which occurs above a caisson during overtopping. Input data consists of wave and breakwater structural conditions, as well as water depth in front of the caisson.

The green wave stage is characterized by the overtopping wave front having a parabolic trajectory. The distance between the caisson's seaward edge and the crash point of the wave front is called the "green wave range," and is represented by l_3 . The value of l_3 is determined by the velocity of the rising wave crest (wave crest rise velocity) above the caisson's seaward edge and the wave velocity. The maximum water depth and current velocity are considered to be constant within the green wave range.

In the overtopping flow stage, the maximum water depth above the crown changes over time, i.e., it decreases within a certain distance from the seaward edge, called the "accelerated flow range," then tends to be almost constant, called the "constant flow range." The maximum current velocity in the former range increases as the wave approaches the landward side, becoming nearly uniform in the latter range. In the model, η_1 represents the maximum water depth at the top of the caisson's seaward edge, while l_1 represents the horizontal distance over which the water depth changes.

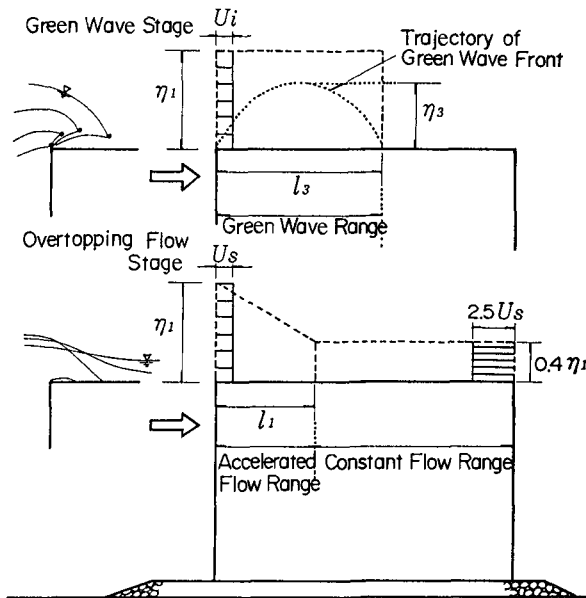


Figure 3 Overtopping wave model

3. 1 Green Wave

3.1.1 Wave Crest Rise Velocity

The rise velocity of the overtopping wave crest at the moment it runs up above the crown, V_{sf} , is equal to the vertical velocity of the wave's surface profile. V_{sf} can be evaluated using a second-order approximation formula for finite amplitude standing waves. If the breakwater superstructure is the composite type, the effects of its rubble mound must be considered because they differ depending on wave length L and mound shape. It is reasonable to consider that the mound has a significant effect on waves when the mound shoulder width, B_M , is relatively large in comparison with L , and also that the mound has only a slight effect when B_M is relatively small. Thus, use of the ratio B_M/L enabled us to develop a functional formula for obtaining the representative water depth hm , which subsequently determines overtopping wave motion, i.e.,

$$\begin{aligned}
 hm = d & & : B_M/L \geq 0.16 \\
 d + (h - d) \frac{0.16 - B_M/L}{0.05} & & : 0.11 < B_M/L \leq 0.16 \\
 h & & : B_M/L < 0.11
 \end{aligned} \tag{1}$$

where h is the natural water depth in front of the breakwater and d is the water depth above the rubble mound.

Figure 4 shows the relationship between B_M/L and V_{sf} using Eq. (1), where the experimental and calculated values clearly indicate good agreement.

Overtopping waves move landward as soon as they run up over the crown, and at this moment, the wave crest horizontal velocity at hm has a proportional relation with wave velocity C_m , i.e., it is about 30% smaller than C_m regardless of crown height. Thus, if we consider the motion of the front to be in free-fall, having come over the caisson's seaward edge at V_{sf} with a horizontal velocity of $0.3C_m$, then a functional formula can be developed to determine the trajectory of the green wave front, with l_3 being subsequently expressed as

$$l_3 = 0.6C_m \cdot V_{sf}/g, \tag{2}$$

where g is gravitational acceleration.

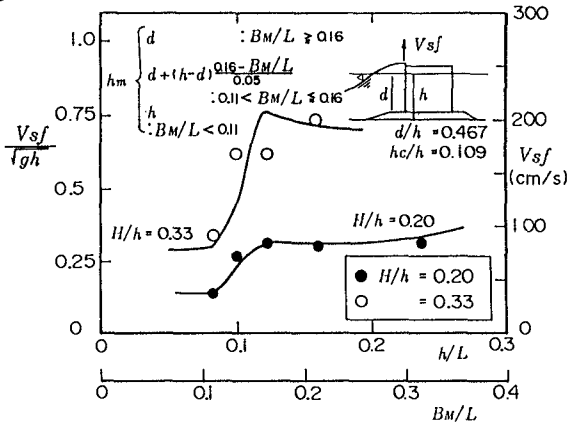


Figure 4 Relation between B_M/L and V_{sf}

3.1.2 Maximum Water Depth and Current Velocity

The distribution of the maximum water depth in the green wave stage is considered to be constant within the green wave range, being equal to the overtopping flow stage's maximum water level η_1 at the caisson's seaward edge. Experiment results enable the corresponding maximum current velocity, U_i , to be expressed as a function of Cm and wave height H , i.e.,

$$U_i = 0.8Cm(1.67H/hm - 0.67)^{1/3} \quad : H/hm \geq 0.4 \quad (3)$$

$$0 \quad : H/hm < 0.4$$

3.2 Overtopping Flow

3.2.1 Maximum Crest Height over The Caisson's Seaward Edge

Goda et al.³⁾ developed the following formula for determining the wave crest height ratio K for standing waves, being the ratio of the run-up height above the still water level in front of a caisson, R , to the wave height, H :

$$K = \min \left\{ \left[1.0 + a(H/h) + b(H/h)^2/Ksb \right], c \right\}, \quad (4)$$

where Ksb is the coefficient expressing nonlinear shoaling effects and breaker decay, while $(a, b, c) = (1.0, 0.8, 10.0)$ for vertical walls. K is 1.0 for small amplitude standing waves and exceeds 1.0 as their finite amplitude increases. The second term in the brackets of Eq. (4) represents the effect in which K increases in proportion to H/h under the condition that no breakers exist, while the third term represents a green wave generated in front of the caisson by breakers. When breaking waves hit the caisson, overtopping waves run up high above it and produce splashing. The quantity of splashed water, however, is relatively small; thus we neglected the third term.

In general, breakwaters can handle large quantities of water from overtopping waves, and because wave overtopping reduces the value of the reflection coefficient, K tends to become constant and is not proportional to H per Eq. (4). We therefore included the effect of overtopping waves using the following formula:

$$K = 1 + \alpha_1 H/hm \quad : H/hm < \frac{-1 + \sqrt{1 + 4\alpha_1 hc/hm}}{2\alpha_1}$$

$$\frac{1 + \sqrt{1 + 4\alpha_1 hc^*/hm}}{2} \quad : H/hm \geq \frac{-1 + \sqrt{1 + 4\alpha_1 hc/hm}}{2\alpha_1} \quad (5)$$

$$hc^* = hc \frac{H/hm}{2H/hm - \frac{-1 + \sqrt{1 + 4\alpha_1 hc/hm}}{2\alpha_1}} \quad (6)$$

The resultant K values enable calculating the maximum wave crest run-up height at the caisson's seaward edge, i.e.,

$$\eta_1 = K \cdot H - hc, \quad (7)$$

where hc is the breakwater crown height and α_1 is a correction factor dependent on the breakwater structure. For a composite breakwater, $\alpha_1 = 1.0$; whereas $\alpha_1 = 0.5$ for a breakwater covered with wave-dissipating blocks or a slit-caisson breakwater.

Figure 5 shows the experimental (when overtopping occurred) and calculated (Eq. (5)) K values for Experiment A, where the experimental values ranged from 0.9 to 1.1 when $hc/h = 0.109$, and from 1.0 to 1.2 when $hc/h = 0.207$: results that confirm a higher crown height will increase K . In addition, when overtopping waves

occurred, the values calculated using Eq. (5) tended to be constant and independent of changes in wave height, being in good agreement with the experimental values.

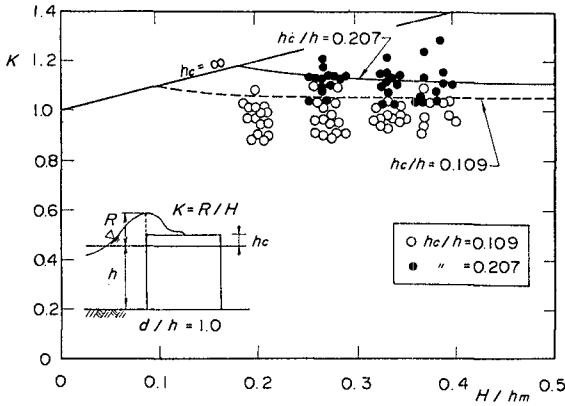


Figure 5 Wave crest height ratio

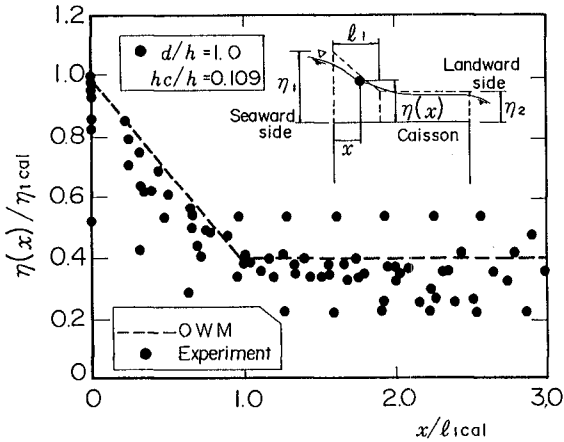


Figure 6 Distribution of maximum water depth above a caisson

3.2.2 Maximum Water Depth

The accelerated flow range l_1 can be expressed as a function of hc , maximum water depth η_1 , and wave velocity Cm . The maximum water depth in the constant flow range is known to be about 0.4 times smaller than η_1 at the caisson's seaward edge, and therefore, the maximum water level at an arbitrary crown point $\eta(x)$ can be calculated using the values of η_1 and l_1 occurring during overtopping flow stage, i.e.,

$$\eta(x) = \begin{cases} \frac{l_1 - 0.6x}{l_1} \eta_1 & : x < l_1 \\ 0.4\eta_1 & : x \geq l_1 \end{cases} \quad (8)$$

Figure 6 shows the distribution of experimental and calculated maximum water levels above the crown of a vertical breakwater with $hc = 8.2$ cm ($hc/h = 0.109$), in which the water depth and distances from the caisson's seaward edge are respectively non-dimensionalized by η_1 and l_1 . Note that the experimental values are scattered, and also that when $x/l_1 = 0$, η/η_1 ranges from 0.8 to 1.0, becoming 0.25 to 0.55 in the constant flow range. Since the experimental values are roughly dispersed around the calculated ones, this indicates good agreement.

3.2.3 Maximum Current Velocity

Since our Experiments A clarified that the current velocity in the overtopping flow stage has a relationship with water depth, and also that their maximum values have only a slight phase difference, this indicates the maximum current velocity $U_s(x)$ can be determined by dividing the maximum overtopping wave quantity q_{max} by $\eta(x)$ (Eq.(8)). Based on a formula modeling steady flow in a dam, we used tests to examine the flow coefficient C_1 , which enables calculation of the overtopping wave quantities. Consequently, a functional formula was developed to obtain q_{max} , i.e.,

$$q_{max} = (0.68 + 1.10 \cdot H/hm)C_1\eta_1^{3/2} \quad : H/hm < 0.4$$

$$\left(0.8 + \frac{0.32}{(10H/hm - 4)^2 + 1} \right) C_1\eta_1^{3/2} \quad : H/hm \geq 0.4 \quad (9)$$

where $C_1 = 1.61$ ($m^{0.5}/s$).

Figure 7 shows the distribution of the maximum current velocity above the caisson for $d/h = 1.0$ and $hc/h = 0.109$. The x-axis is the distance from crown's seaward edge, x , divided by l_1 , while the y-axis is the maximum current velocity at each point, $U_s(x)$, divided by the maximum current velocity in the constant flow range, $U_{scal}(\infty)$. When x/l_1 is less than 1.0, i.e., within the accelerated flow range, the experimental current velocity increases as x increases. It is clear that in the constant flow range, the value of $U_s(x)/U_{scal}(\infty)$ tends to be constant, ranging from 0.9 to 1.15. Note the rough agreement between experimental and calculated values.

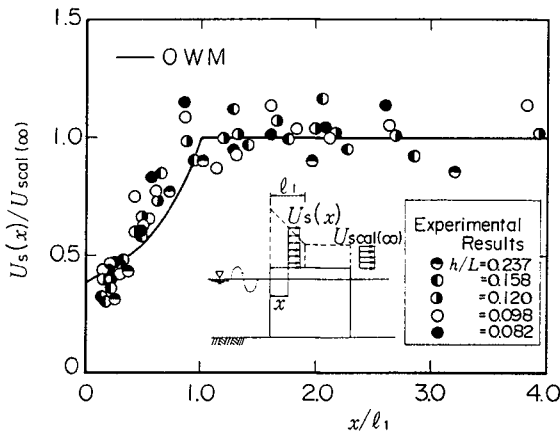


Figure 7 Distribution of maximum current velocity above a caisson

4. FORMULA FOR WAVE FORCE ACTING ON HANDRAILS

Overtopping wave forces acting on column-shaped handrail members may include: (i) an impulsive wave force that occurs when an overtopping wave hits, and (ii) a drag force that is dependent on the current velocity of overtopping waves. Because these members have relatively small diameters, the impulsive component was assumed to be negligible, and therefore, only the drag force was considered. Neglecting the effect of impulsive pressure was confirmed to be appropriate using field experiments. The drag force can be expressed as

$$F = \frac{w_0}{2g} C_D \cdot A \cdot U_{max}^2, \tag{10}$$

where A is the horizontally projected area of a submerged handrail at the maximum water depth, C_D is the drag coefficient, and U_{max} is the maximum current velocity estimated to occur at the handrail installation point. We used the largest values of U_{max} observed in the green wave and overtopping flow stages.

Figure 8 shows the ratio of experimental to calculated wave forces, F_{exp}/F_{cal} , acting on a handrail. Wave forces acting on handrail members installed on the caisson's seaward and landward edge are indicated. Since the handrail was made of cylindrical column-shaped members, we assumed $C_D = 1.0$. At the seaward edge, the maximum current velocity in the green wave stage is larger than that in the overtopping flow stage, and consequently, the wave forces at this edge were calculated using the maximum velocity U_i in the green wave stage. Since the landward edge is in the constant flow range outside the green wave range, we used the maximum current velocity U_s . At the seaward edge handrail, F_{exp}/F_{cal} ranged from 0.7 to 1.2, with good agreement being present between experimental and calculated values. At the landward edge handrails, F_{exp}/F_{cal} was slightly less (0.4 to 0.7), which indicates that calculated values are comparatively slightly larger. These experimental results confirm that Eq.(10) is suitable if $C_D = 1.0$ for cylindrical column-shaped members.

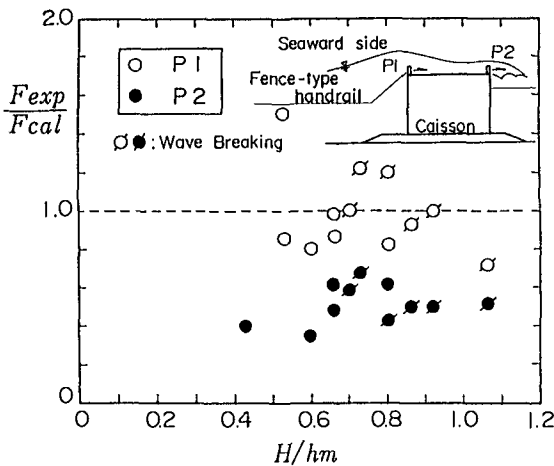


Figure 8 Wave forces acting on a model handrail

At a high Reynolds number, Re , however, the C_D value is lower for this type of handrail. Consequently, since Re values are higher in the field than in experiments, a possibility exists that C_D is actually less than assumed. It should be realized that the characteristics of impulsive wave forces could not be determined because the experimental response characteristics of handrail members did not agree with field results, possibly being due to measuring the wave forces with strain gages. This problem led to using field experiments to examine the characteristics of wave forces and impulsive wave forces (Section 5).

5. FIELD EXPERIMENTS

5.1 Background

5.1.1 Location of Field Experiments

Field experiments were conducted from November 1991 to March 1992 above the Second North Breakwater of Sakata Port in northeastern Japan. **Figure 9** shows plane and cross-section views of the field site. Although this front-line breakwater is installed in deep water (≈ 16 m), its crown height is relatively low (4.5 m) because it was under construction during the tests. The upper seaward edge of the caisson has a 45° slope. An observation house was built about 2 km away from the test breakwater to record measured data transmitted through optical fiber cables.

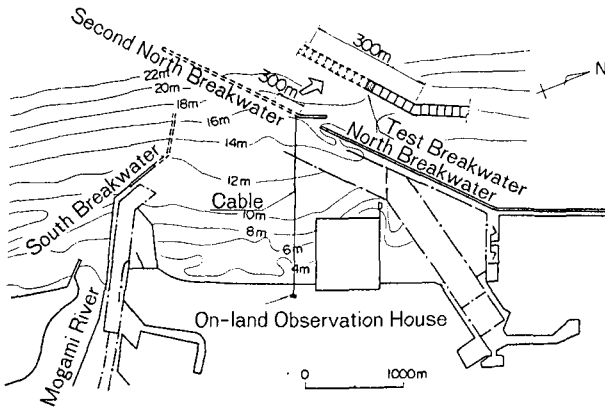


Figure 9 (a) Plane view of Sakata Port

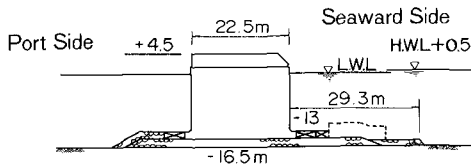


Figure 9 (b) Cross-section view of test breakwater

Table 1 Stanchion shapes

Name	Shape	Diameter (mm)	Thickness (mm)	Allowable wave height (m)
A1	Round steel pipe	216.3	8.2	-----
B1-4	Round steel pipe	101.6	4.2	-----
C1-4	Round steel pipe	48.6	3.2	10
D1	Square steel pipe	100	4.5	-----
E1	Square steel pipe	75	4.5	-----
a	Round steel pipe	27.7	2.3	4.6
b	Round steel pipe	76.3	3.2	14.8
c	Round steel pipe	139.8	4.5	-----
d	Round steel bar	13	---	4
e	Round steel bar	25	---	7.7
f	Round steel bar	38	---	12.3
g	Round steel bar	48	---	-----
F1	Fence-type	60.5	3.2	4
F2	Chain-type	114.3	6	-----

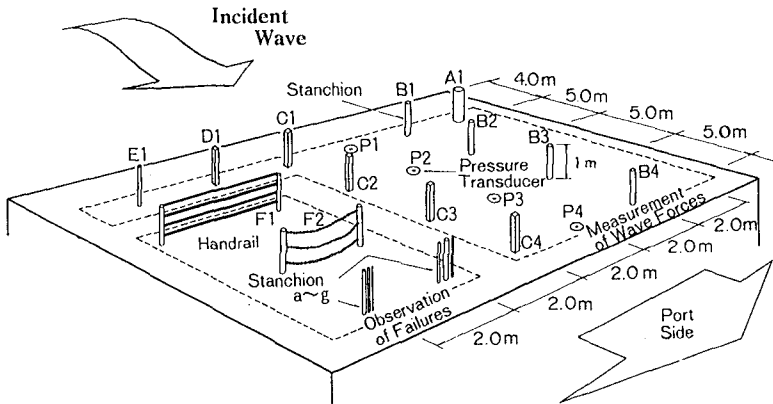


Figure 10 Field experiment setup

5.1.2 Experiment Outline

A wave force measurement test and failure test were carried out in the field. For the wave force test, five kinds of test stanchions (1-m-tall, round or square steel pipes) were installed on the breakwater crown (**Table 1**), and we measured the strain generated at their bottoms. **Figure 10** shows the employed stanchion setup. Stanchions of each type (*A1-E1*) were installed 4 m away from the seaward edge. Stanchions *B* and *C* were also installed 9, 14, and 19 m away from the seaward edge.

For the failure test, we installed conventionally used fence- and chain-type handrails (*F1* and *F2*), round steel pipes (*a-c*), and round steel bars (*d-g*) in order to observe tilt angles and other failure conditions that can occur after a major storm (**Table 1**, **Fig. 10**). Wave pressure, current velocity, and wave height were obtained corresponding to when the bottom of a stanchion reaches allowable stress. The fence-type handrail (*F1*) had an allowable wave height of only 4.0 m, which indicates that it will fail at comparatively low wave heights.

To examine the motion characteristics of overtopping waves above the crown, we installed four pressure transducers (*P1-4*) at various locations on the crown. Water depth during an overtopping wave was determined by removing the impulsive component from vertical pressure, i.e., only the static pressure component was used to obtain water depth. We calculated the current velocities during overtopping waves using phase differences in the pressure profiles.

5.1.3 Analysis Method

By assuming the wave pressure acting on the test stanchions is equally distributed, we could calculate strain-produced pressure. Peak pressures were then compared with observed maximum wave heights. These heights were measured about 250 m away from the breakwater along its normal line; hence some errors may arise when evaluating the wave pressure characteristics. Wave direction data was obtained about 7 km directly seaward of the breakwater, being a location where good correlation is present.

5.2 Wave Forces Acting on Handrails

5.2.1 Typical Strain and Water Pressure Profiles

Figure 11 shows typical profiles of the strain which occurred at the bottom of the test stanchions and those of water pressure in response to a maximum wave height of 7.4 m ($hc/H_{max} = 0.50$) (January 24, 1992, 8:14-8:34a.m.). Strain profiles for stanchions *A1*, *B1-4*, *C1-2*, and *D1* are shown with water pressure profiles from *P1-4*. The maximum water depth calculated from the water pressure profiles is 3.2 m at *P1*, the most seaward point, and 1.2 m at *P4*, the most landward point, which indicates that the water depth exceeded the height of the stanchions over the entire the crown area. The average current velocity determined from the phase difference of these maximum water levels is 9.1 m/s between *P1* and *P2*, 11.1 m/s between *P2* and *P3*, and 12.5 m/s between *P3* and *P4*, showing a slight increase toward the landward edge.

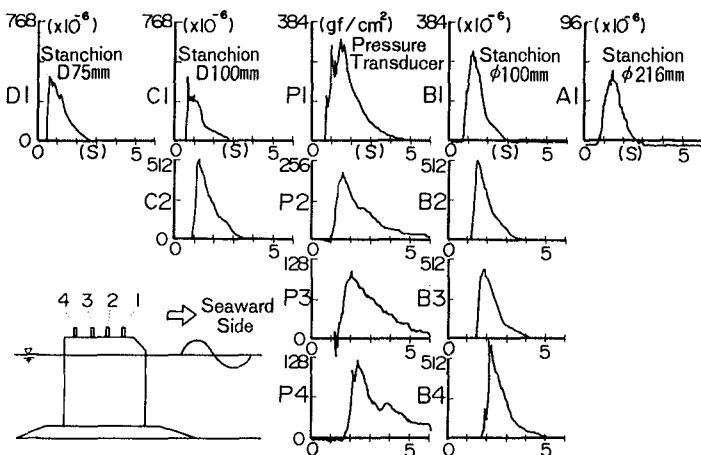


Figure 11 Strain and pressure profiles

As can be seen in *C1*'s profile, strain in the stanchion includes both impulsive and drag force components. The impulsive component seems to occur when a portion of an overtopping wave smashes into the stanchions. Its pressure profile is a strong, sharp peak acting over a relatively short time. In comparison, the drag force component is dependent on current velocity, displaying a relatively mild peak acting over a long time. With the exception of *C1*, the profiles of *C2*, *A1*, and *B4* indicate the presence of an impulsive component, although it is much smaller than the drag force.

Regarding the drag force component of strain, similar to current velocity, strain increased toward the landward edge, e.g., the non-dimensional wave pressure, p/w_oH , at *B1-4* was respectively 0.28, 0.47, 0.46, and 0.57.

The stanchion shape also affected the wave force acting against it. If we compare the drag force component of p/w_oH at the most seaward stanchions, the cylindrical column-shaped ones (*A1* and *B1*) had values of 0.2 and 0.28, whereas those of the square-column ones (*C1* and *D1*) were twice as large at 0.42 and 0.45. This result suggests a difference occurs in the drag coefficient.

5.2.2 Wave Pressure Acting on Stanchions

Figure 12 shows the wave pressure acting on stanchion *B1* in the form of the non-dimensional wave pressure p/w_oH , where peak values of the drag force component and of any impulsive component are indicated. Although the data is scattered due to the effects of different tide levels and wave directions, at a maximum wave height of 6 m or greater, p/w_oH ranges from 0.25 to 0.4 for the drag force component and from 0.3 to 0.5 for the impulsive component. Similarly, the drag force component of the pressure ranges from 0.2 to 0.6 for the cylindrical column stanchions and from 0.3 to 1.0 for the square column stanchions, though the degree of scattering varies with position.

Since impulsive wave pressures vary with position depending on the overtopping wave conditions, as well as showing great variations in scale, peak impulsive pressures were compared with peak drag pressures as shown in **Fig. 13**. The x-axis indicates drag pressures P_s , while the y-axis indicates P_n , the peak values

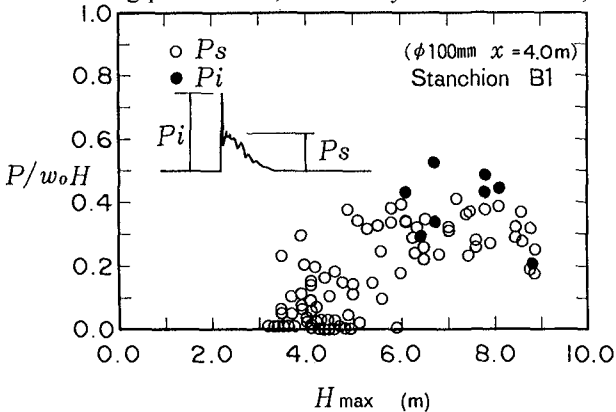


Figure 12 Non-dimensional wave pressure acting on stanchion B1

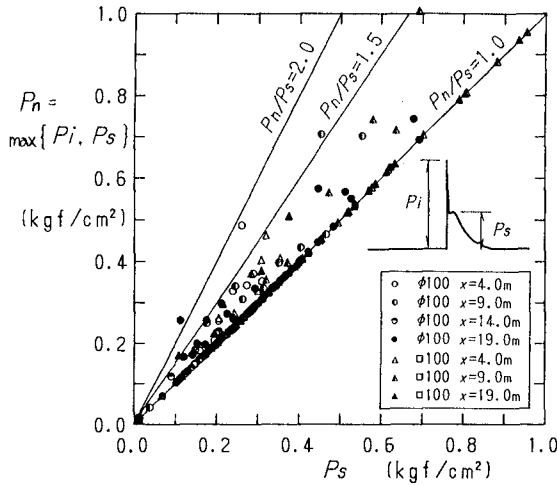


Figure 13 Impulsive pressure

of P_s and impulsive pressure P_i . When P_n/P_s equal to 1.0, the peak pressures are caused by the drag force component, whereas when greater than 1.0, they are caused by the impulsive component. Although the maximum P_n/P_s value is around 2.0, it generally is less than 1.5; hence, impulsive pressures do not generally exceed the drag pressures by much. In addition, the impulsive pressures measured at the stanchions were less frequent and smaller than those measured by pressure transducers located the same distance away from the seaward edge. The relatively small impulsive pressures observed on stanchions may be due to their thin columnar shape or a dynamic response at their natural frequencies (1.5-7 Hz). Measured impulsive wave pressures are expected to be conservative in comparison to those on actual handrails, because actual handrails have the same quality and are fabricated from same material as the test stanchions, and also their natural frequencies are slightly less due to no transverse members being present. Therefore, neglecting impulsive wave pressures during handrail design, as is done in the conventional breakwater design method, is considered acceptable.

5. 3 Comparison with Wave Force Formula

5.3.1 Comparison Between Measured and Calculated Wave Forces

Figure 14 compares measured and calculated wave forces, where the x-axis indicates the non-dimensional value of l_1 divided by the distance x away from the caisson's seaward edge, and the y-axis indicates the ratio of the measured wave force F_m to the calculated one F_c . For the measured wave force, only the drag force component was included, and for the calculated force, a C_D value of 1.0 and 2.0 was used for the cylindrical and square stanchions, respectively. As shown, in a relatively seaward area where x/l_1 is less than 1.0, the measured forces for the cylindrical and square columnar stanchions are only 40-90% of their calculated forces (ave.≈60%). On the other hand, in a relatively landward area where x/l_1 is greater than 1.0, the

F_m/F_c values are close to 1.0 on the average, though they are widely scattered from 0.3 to 1.5. These results confirm the calculated values are roughly suitable.

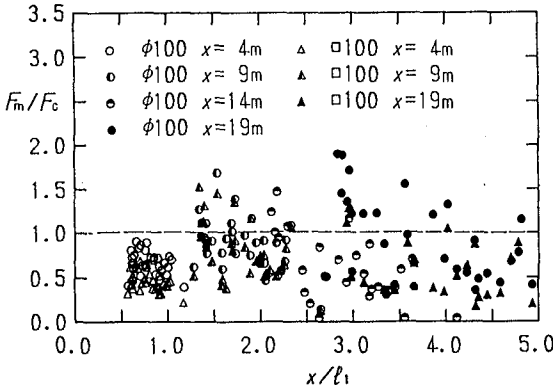


Figure 14 Comparison of measured and calculated forces acting on stanchions

5.3.2 Reproducing Failure Conditions Using Calculated Stress

Structures that tilted or completely fell over during the experiment are: stanchion *E* used in the wave force measurement; and stanchions *a*, *d*, *e*, and handrail *F1* used in the failure test. Since the allowable wave heights for all these damaged members is 10 m or less (Table 1), these failures could easily be predicted by wave observation results. The strongest storm during the experiment produced a maximum wave height of 10.5 m (Dec. 28-30, 1991), and stanchion *e* was tilted. Stanchions *a*, and *d* and handrail *F1* failed in a storm on Nov. 19-21, 1991.

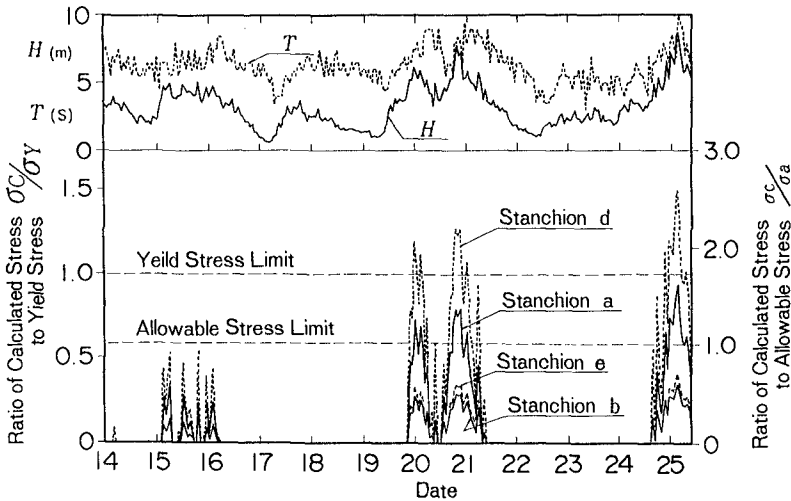


Figure 15 Comparison of calculated and allowable stresses at the bottom of stanchions

Figure 15 shows wave conditions and calculated stresses at the bottom of several stanchions from Nov. 14-25, 1991. We examined damaged stanchions *a* and *d* and undamaged stanchions *b* and *e*. The wave condition data was used to determine calculated stress σ_c , which was non-dimensionalized by dividing with either allowable stress σ_a or yield stress σ_y .

When wave forces act on a stanchion, the stresses generated in it are generally the greatest at the bottom. When the stresses there exceed allowable stresses, i.e., $\sigma_c/\sigma_a > 1.0$, a greater possibilities exists for tilting or other failures to occur. From Nov. 14-25, two major storms produced maximum wave heights of 5.0 m greater, with one wave having a maximum height of 8.8 m. During storms before Nov. 19, stanchions *a* and *d* both had $\sigma_c/\sigma_a < 1.0$, and no failure took place. However, when their maximum σ_c/σ_a ratios increased to 1.4 and 2.1 during the Nov. 19-22 storms, both suffered failure. In addition, their maximum value of σ_c/σ_y increased to 1.5 and 0.75. In contrast, both these ratios for stanchions *b* and *e* were less than 1.0, and they were not damaged. For the fence-type handrail *F1*, which failed during same period, $\sigma_c/\sigma_y > 1.5$. These results indicate that the stress calculated using Eq. (10) is accurate enough to be used to the practical design.

6. CONCLUDING REMARKS

We have shown that the motion of an overtopping wave above a caisson can be classified two distinct stages: the "green wave" and "overtopping flow" stages. The fundamental characteristics of each stage were also classified, which enabled developing a model of the motion. Our resultant model can effectively determine maximum water depth and the maximum current velocity above a caisson.

Through the field experiments using handrails, it was possible to understand the effects of impulsive wave forces and the practical wave force characteristics in the region of high Reynolds numbers. It also was possible to estimate the wave force acting on a breakwater handrail as a drag force and to verify the appropriateness of the estimation through wave force measurement and failure tests.

ACKNOWLEDGMENTS

Sincere gratitude is extended to Dr. Tomotsuka Takayama, Director of the Port and Harbour Research Institute for his valuable advice and encouragement.

REFERENCES

- 1) Takahashi, S., Endoh, K., and Muro, Z. : Experimental study on motions and forces of overtopping waves, Rept. of Port and Harbour Res. Inst. Vol.31, No.1, 1992, pp.3-50. (in Japanese)
- 2) Sugawara, K., et. al. : Experimental study of wave forces acting on handrails on breakwaters, 39, pp.716-720. (in Japanese)
- 3) Goda, Y., et. al. : Laboratory investigation on the overtopping rate of seawalls by irregular waves, Rept. of Port and Harbour Res. Inst. Vol.14, No.4, 1975, pp.3-45. (in Japanese)